PERGAMON

Mechatronics 9 (1999) 95–110

MECHATRONICS

Frequency reshaped quadratic control of a low-cost human-level performance belt-driven robot

Kok-Meng Lee*, Chad Rutherford

George W. Woodruff School of Mechanical Engineering, Georgia Institute of Technology, Atlanta, GA 30332-0405, U.S.A.

Received 7 November 1997; revised 13 July 1998; accepted 31 July 1998

Abstract

Belt-driven robots are desirable for many industrial applications that require a fast response for a relatively large amount of travel in a system. A belt-drive is a simple, lightweight device that is also cost effective in comparison to other methods of arm positioning. The tradeoff of a belt-driven robot is the need for an effective control strategy to reject time-varying disturbances due to the belt stiffness variation and the presence of resonance excited by disturbances of high frequencies. In this paper, we present the dynamic model and control of a low-cost belt-driven robot.

We present here the modeling and control of an intelligent integrated belt-driven manipulator (IIBM) developed at Georgia Tech. The belt-driven robot is a low-cost human-level performance robot, specifically meant to meet or exceed the performance of a human taking shrink wrapped packages off a conveyor and placing them in a basket for delivery. Therefore, such attributes as speed and accuracy are dictated by the level of performance a human can achieve. The control design for the IIBM presents a challenge in that a control system for the belt-driven axis must be designed by using a low-order plant model that is robust enough to variations in both the parameter changes and the un-modeled high frequency dynamics. For these reasons, we investigate the use of frequency reshaped linear quadratic (FRLQ)) control in the development of a low-cost IIBM, which combines the time domain linear quadratic optimal control design with classical frequency response methods.

The control strategy, based on the FRLQ method, has been implemented on the first axis of an IIBM. The performance has been evaluated analytically by simulation and experimentally, the results of which are compared against the control system originally used by the IIBM designers, a well-tuned PD controller. Experimental implementation has demonstrated that the frequency reshaped linear quadratic control has a potential to significantly improve the performance of the belt-driven robot.

* Corresponding author. Tel.: +1 404 894 7402; fax: +1 404 894 9342; e-mail: kokmeng.lee@me.gatech.edu

0957–4158/99/$—see front matter
PII: S0957–4158(98)00042–7

1. Introduction

The increased demand for poultry products has been a driving force for automation in plants across the U.S., and is being influenced by several factors, including production control, output consistency, and the desire to remove humans from hazardous working conditions. Automation has already done a great deal in increasing the efficiency of poultry plants. One study [1] shows that labor efficiency has improved from 57 birds per h in 1967 to 240 per h in 1991. The food processing and packaging industry, however, lags far behind other types, such as chemical and automotive industries, in terms of automation. The reason for this is that the poultry industry faces unique challenges, such as the following: (1) Unlike other areas, where robots operate on identical parts, poultry segments such as chicken breasts, thighs, and legs vary in size and shape, making automation of poultry processing lines difficult. (2) Any robot or actuator used to handle or otherwise interact with food products must pass certain requirements set by the Food and Drug Administration. These hygiene requirements are not necessary in other industries. (3) In order to justify the need for automation from a cost-saving viewpoint, robots must perform the repetitive task in a shorter amount of time, and with more accuracy than a human. To address these automation needs of the poultry industry, researchers at Georgia Tech. [2] have endeavored a new design paradigm of robots, known as human-level performance robotics. As a proof of concept, their efforts have led to the development of an intelligent integrated belt-driven manipulator (IIBM).

We present here the modeling and control of the IIBM developed at Georgia Tech. [2]. The IIBM is a low-cost human-level performance robot, specifically meant to meet or exceed the performance of a human taking shrink wrapped packages off a conveyor and placing them in a basket for delivery. Therefore, attributes such as speed and accuracy are dictated by the level of performance a human can achieve. Belt-driven actuators are used in IIBM since it requires a fast response for a relatively large amount of travel in a system. A belt-drive is a simple, lightweight device that is also cost effective in comparison to other methods of arm positioning. The tradeoff of a belt-driven robot is the need for an effective control strategy to reject time-varying disturbances due to the belt stiffness variation and the presence of resonance that could be excited by disturbances of high frequencies.

Several control schemes have been proposed in the literature which address the control of robotics with flexible joints (e.g., Mills [3], Wang and Liu [4]). The control design for the IIBM presents a challenge in that a control system for the belt-driven axis must be designed by using a low-order plant model that is robust enough to variations in both the parameter changes and the unmodeled high frequency dynamics. For these reasons, we investigate the use of frequency reshaped linear quadratic (FRLQ) control in the development of a low-cost IIBM, which combines the time domain linear quadratic optimal control design with classical frequency response methods.

The FRLQ control problem was originally formulated and solved [5] using state space methods, expressing the time dependent performance index in the frequency domain, and allowing the heretofore constant weighting matrices to become frequency

dependent. This allowed the designer to penalize not only certain states, outputs, or control inputs, but also specific frequency regions of these elements. The design was therefore much more flexible, and had several positive results. Since 1980, much research has been done on the FRLQ method. Anderson and Mingori [6] studied the robustness characteristics of the method, and concluded that, when high frequencies are weighted more heavily than low frequencies, passband robustness is lessened while stopband robustness is improved. Imai et al. [7] studied the effects of FRLQ control as applied to the problem of disturbance attenuation, and developed a method of designing the return-difference-matrix by adjusting the weighting matrices. The FRLQ control, however, requires that the harmful frequency or frequencies must be known prior to control. In order to predict the frequency range, a high order dynamic model of an IIBM has been developed, which is essential to optimal design, analysis and control of a belt-driven robot. In this paper, we present the dynamic model and control of a low-cost belt-driven robot. Experimental implementation has demonstrated that the frequency reshaped linear quadratic control has a potential to significantly improve the performance of the belt-driven robot.

The remainder of this paper is organized as follows: Section 2 provides an overview of the IIBM system. The dynamic model of the IIBM is then given in Section 3. Section 4 presents the frequency reshaped control algorithm for the IIBM, the results of the simulation and experimental implementation are given in Section 5. Finally, the conclusions are drawn in Section 6.

2. System overview

Figure 1 shows a typical poultry handling task, where a woman is removing chicken packages from a conveyor and loading them on a basket for delivery to another region of the factory. Automation is often desired for this type of task due to

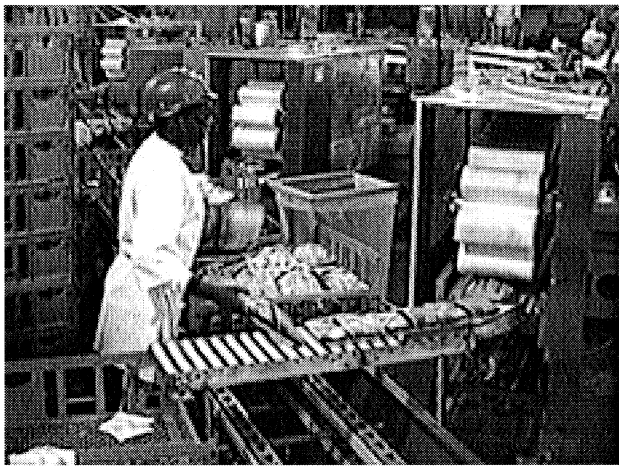

Fig. 1. Typical factory floor of a poultry processing plant.

workplace hazards, both environmental and ergonomic. To meet or exceed the human level performance, the first axis of the handling robot must be designed to travel horizontally 22 in (0.5588 m) in at most 0.5 s. This step response should have no more than 5% overshot and a steady state error of no more than 1/8th in (31.7 mm) for this travel.

The three degree-of-freedom (DOF) low-cost IIBM to automate this particular task is shown in Fig. 2. The first axis joint consists of two aluminum pulleys, upon which rides a stainless steel belt. A wash-down permanent magnet brush-less motor drives one pulley, and the rotational motion is converted to translation motion through the belt. The second and third axes are housed in a hollow cylinder which is attached to the belt and rides along the horizontal axis via a linear bearing. The second axis provides the rotational motion, while the third is the source of vertical motion. The chicken packages are lifted by four vacuum tubes on the end effector.

Because of the length of travel involved, the first axis is the most time critical component of the IIBM. A HP 3562A dynamic signal analyzer was used to determine the system's transfer function for this axis experimentally. The input to the system is the voltage applied to the first axis motor, which is connected to the first pulley via a gear box. The actuator systems for the second and third axes and the end-effector were treated as one lumped mass. The position of this mass is the plant controlled variable, $x(t)$. For safety reasons, the test was discontinued when the system experienced a resonance at 6 Hz. Within this limited range, the open-loop transfer function of the belt-driven actuator was experimentally determined for a limited range to be

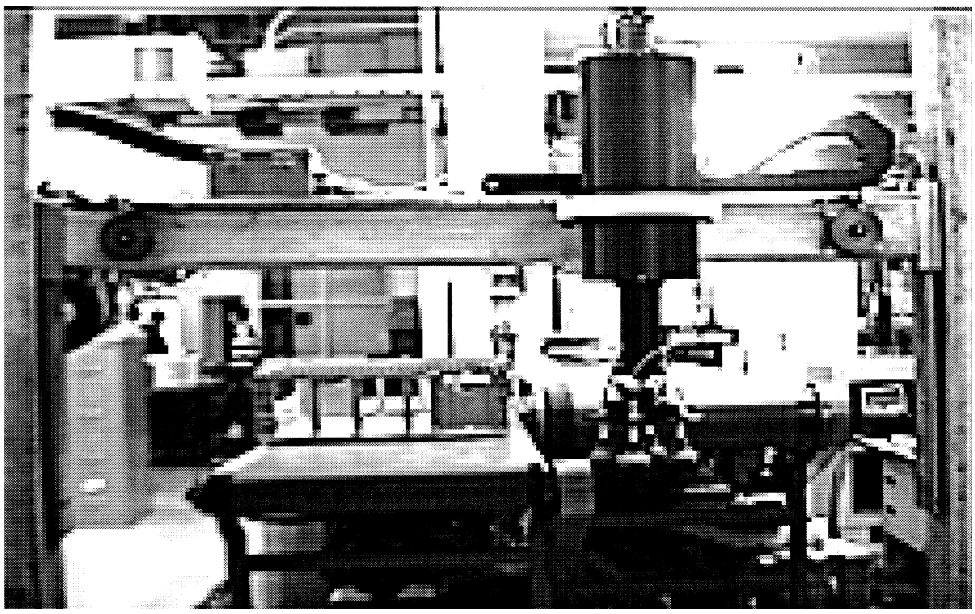

Fig. 2. Intelligent integrated belt manipulator (IIBM).

$$G(s) = \frac{9.1095}{s(s+25.133)} \tag{1}$$

3. Dynamic model

In order to provide a better understanding of the IIBM belt-drive system, a dynamic model was constructed using the lumped parameter approach. Figures 3 and 4 are illustrations of the modeled system. Figure 3 consists of the first axis motor, two pulleys, the belt modeled as three springs in series, and the lumped mass M. This mass which represents the second and third axes and the end-effector is connected to the belt by a screw, and it rides along a linear bearing mounted on a stainless steel beam (denoted as M_3 in Fig. 4). Figure 4 adds the masses corresponding to the two vertical and one horizontal aluminum beams that make up the IIBM structural system. This addition was necessary because vibrations of the structure were observed during system operation. The system parameters and their values necessary to construct the modeled system are defined in Table 1.

The state space equations, derived from the free-body diagrams in Figs. 3 and 4, are as follows:

$$\begin{bmatrix} \dot{\mathbf{x}}_1 \\ \dot{\mathbf{x}}_2 \end{bmatrix} = \begin{bmatrix} \boldsymbol{A}_{11} & \boldsymbol{A}_{12} \\ \boldsymbol{A}_{21} & \boldsymbol{A}_{22} \end{bmatrix} \begin{bmatrix} \mathbf{x}_1 \\ \mathbf{x}_2 \end{bmatrix} + \boldsymbol{B}u, \tag{2}$$

$$y = x$$

where $\mathbf{x}_i$ and $\boldsymbol{A}_{ii}$ $(i = 1, 2)$ are the state vectors and the system matrices for the belt-drive system and the supporting structure respectively; and u is the voltage input to the motor. The state variables of the belt drive system are

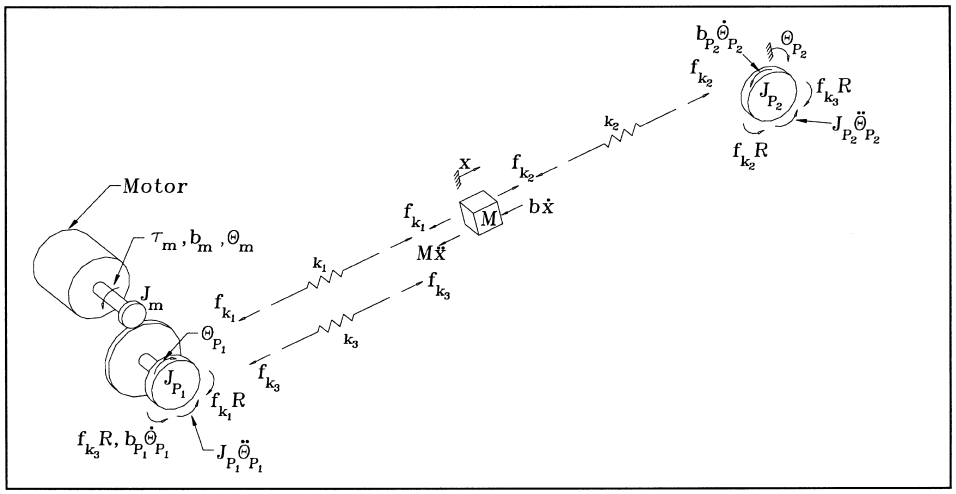

Fig. 3. Model of the IIBM' first axis.

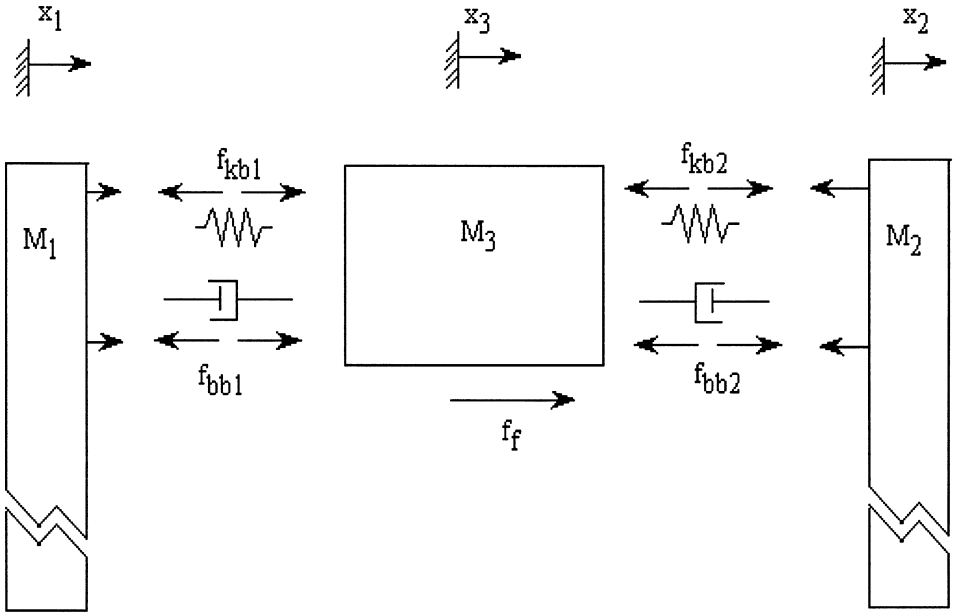

Fig. 4. Model of the IIBM structure.

$$\mathbf{x_1} = [i_a\ \theta_{p1}\ \omega_{p1}\ \theta_{p2}\omega_{p2}\ x\ v]^T;$$

where i_a is the motor current, θ_{pi} and ω_{pi} $(i = 1, 2)$ are the angular displacements and velocities of the pulleys respectively, x and v are the displacement and velocity of the mass M respectively. The input and system matrices for the belt drive system are given as follows:

$$B = \left[\frac{1}{L_a} 0\ 0 \ldots 0\ 0\right]^T;$$

$$A_{11} = \begin{bmatrix} -\frac{R_a}{L_a} & 0 & -\frac{K_e}{L_a} & 0 & 0 & 0 & 0 \\ 0 & 0 & 1 & 0 & 0 & 0 & 0 \\ \frac{K_t}{J_{\text{eq}}} & -\frac{K_{\text{eq}}}{J_{\text{eq}}} & -\frac{b_{\text{eq}}}{J_{\text{eq}}} & \frac{K_3R^2}{(GR)J_{\text{eq}}} & 0 & \frac{K_1R}{(GR)J_{\text{eq}}} & 0 \\ 0 & 0 & 0 & 0 & 1 & 0 & 0 \\ 0 & \frac{K_3R^2}{(GR)J_{p1}} & 0 & -\frac{(K_2+K_3)R^2}{J_{p1}} & -\frac{b_{p2}}{J_{p2}} & \frac{K_2R}{J_{p2}} & 0 \\ 0 & 0 & 0 & 0 & 0 & 0 & 1 \\ 0 & \frac{K_1R}{(GR)M_4} & 0 & \frac{K_2R}{M_4} & 0 & \frac{-K_1+K_2}{M_4} & -\frac{b_f}{M_4} \end{bmatrix}$$

Table 1
Parameter values for theoretical model

Unit		Value
Motor parameters		
J_m	Inertia (N-m^2)	0.00396
B_m	Damping coefficient (N-m-s/radian)	7.12e-3
R_a	Armature resistance (R_a,ohms)	1.765
L_a	Armature inductance (Henry's)	14.6e-3
GR	Gear ratio (GR)	3.1
K_e	Back emf Constant (V-s/radian)	0.467
K_t	Torque Constant (N-m/amp)	0.468
Pulley parameters		
R	Radius (m)	0.0508
J_p	Inertia (N-m^2)	1.46e-4
B_p	Viscous damping coefficient (Nm-s/radian)	0.01472
Lumped mass parameters		
M	Mass of 2nd and 3rd axes (kg)	14.97
B_f	Viscous damping coefficient of linear bearing (N-m-s/radian)	76.099
Belt parameters (at centre of stroke)		
K_1	Spring constant (N/m (0.6858 m))	1.544e7
K_3	Spring constant (N/m (0.6858 m))	1.544e7
K_2	Spring constant (N/m (1.3716 m))	7.718e6
Structure parameters		
M_1	Mass of 1st vertical beam (kg)	62.79
M_2	Mass of horizontal beam (kg)	51.18
M_3	Mass of 2nd vertical beam (kg)	62.79
b_b	Damping coefficient of structure (kg-m-s/radian)	3.12E-4
K_b	Spring constant of structure (N/m)	2.05E+4
Other parameters		
J_{eq}	Equivalent inertia (N-m^2)	$J_{eq} = J_m + \frac{J_{p1}}{(GR)^2}$
K_{eq}	Equivalent spring constant (N/m)	$K_{eq} = \frac{R^2}{(GR)^2}(K_1 + K_3)$
b_{eq}	Equivalent viscous damping coefficient (Nm-s/radian)	$b_{eq} = b_m + \frac{b_{p1}}{(GR)^2}$

Similarly, the state variables for the structure are defined by

$$\mathbf{x}_2 = [x_3\ v_3\ x_1\ v_1\ x_2\ v_2]^T$$

where x_i and $v_i (i = 1, 2, 3)$ are the displacements and velocities of the supporting beams M_i, $(i = 1, 2, 3)$ respectively. The system matrix for the structure is given by

$$A_{22} = \begin{bmatrix} 0 & 1 & 0 & 0 & 0 & 0 \\ -\frac{2K_b}{M_3} & -\frac{2b_b+b_f}{M_3} & \frac{K_b}{M_3} & \frac{b_b}{M_3} & \frac{K_b}{M_3} & \frac{b_b}{M_3} \\ 0 & 0 & 0 & 1 & 0 & 0 \\ \frac{K_b}{M_1} & \frac{b_b}{M_1} & -\frac{K_b}{M_1} & -\frac{b_b}{M_1} & 0 & 0 \\ 0 & 0 & 0 & 0 & 0 & 1 \\ \frac{K_b}{M_2} & \frac{b_b}{M_2} & 0 & 0 & -\frac{K_b}{M_2} & -\frac{b_b}{M_2} \end{bmatrix}$$

As reflected in the matrices A_{12} and A_{21} given below, the coupling between these supports and the belt-driven actuator is through the viscous friction acting on the linear bearing between the mass M and the horizontal beam M_3.

$$A_{12} = \frac{b_f}{M} \begin{bmatrix} 0 & 0 & 0 & 0 & 0 & 0 \\ 0 & 0 & 0 & 0 & 0 & 0 \\ 0 & 0 & 0 & 0 & 0 & 0 \\ 0 & 0 & 0 & 0 & 0 & 0 \\ 0 & 0 & 0 & 0 & 0 & 0 \\ 0 & 0 & 0 & 0 & 0 & 0 \\ 0 & 1 & 0 & 0 & 0 & 0 \end{bmatrix} = \frac{M_3}{M} A_{21}^T;$$

The Bode plots of the experimental transfer function, and of the modeled system, are given in Fig. 5, which shows that the plant is basically a double integrator with high frequency resonance. The small difference between the two curves in the gain plot is due to the estimation of stiffness and friction parameters in the model. The resonance, caused by the springs, occurs after about 1000 radians/s. Figure 6 shows the Bode plots of the supporting structure with the displacement of the vertical beam x_1 treated as the system output. This diagram shows an additional resonance at approximately 36 radians/s, or 6 Hz. This value agrees with the observation in the previous experiments, in which vibration was observed while a frequency response test was performed.

4. Frequency reshaped control of the belt-driven actuator

Although the belt-drive system has a potential of providing a fast response for this relatively long amount of travel, it presents interesting challenges for control due to the possibility of exciting high-order resonance in the first axis. A frequency reshaped linear quadratic (FRLQ) control is implemented for this design for the following reasons: (1) It is desired to construct a controller from a low-order system model

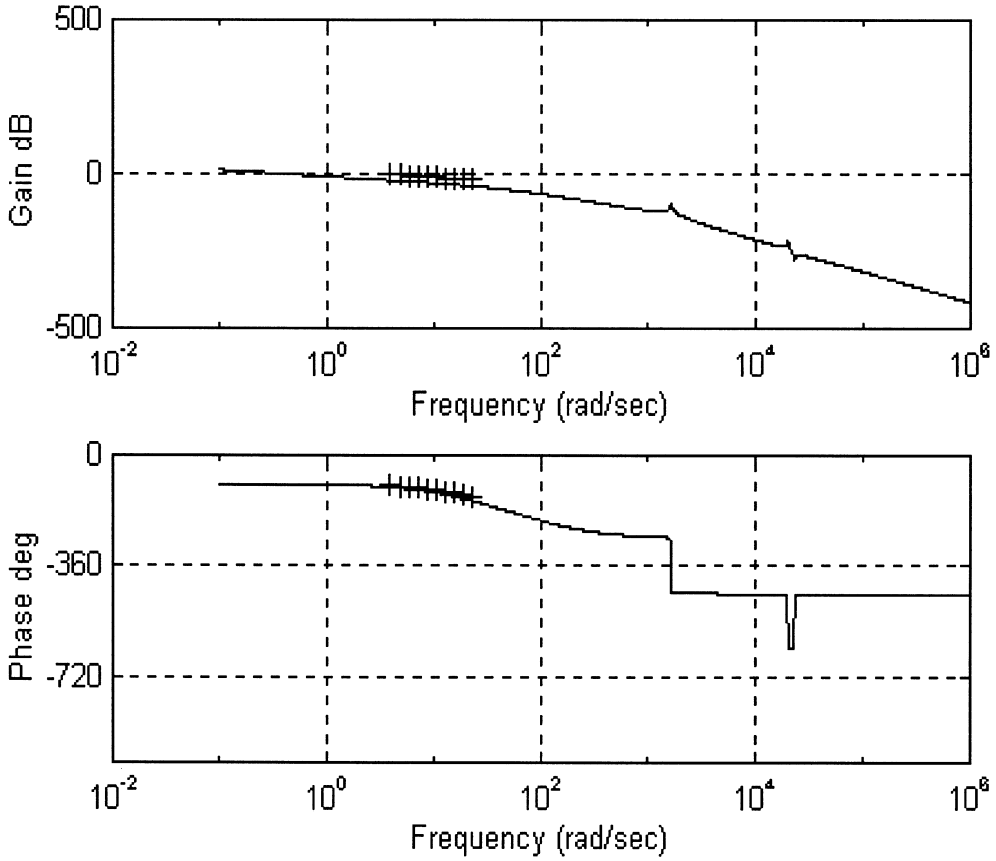

Fig. 5. Open-loop Bode plot of the belt-driven actuator system (solid line-theoretical, crosses—actual data).

which is robust enough to high-order dynamics. (2) The frequency range in which resonance occurs is known. Thus, instead of attempting to minimize for

$$\dot{\mathbf{x}} = \boldsymbol{A}\mathbf{x} + \boldsymbol{B}u$$
$$y = \mathbf{C}\mathbf{x} \tag{3}$$

the performance index

$$J = \int_o^\infty [u^2 + qy^2]\mathrm{d}t \tag{4}$$

we shape the input voltage to the first-axis motor in such a way as to minimize inputs at high frequencies only. Here a simple first order filter is chosen in the performance index to penalize frequencies at or above the first resonance, according to the theoretical models. If the system exhibited resonance at only one frequency or a small range of frequencies, then a notch filter that penalized only that particular frequency

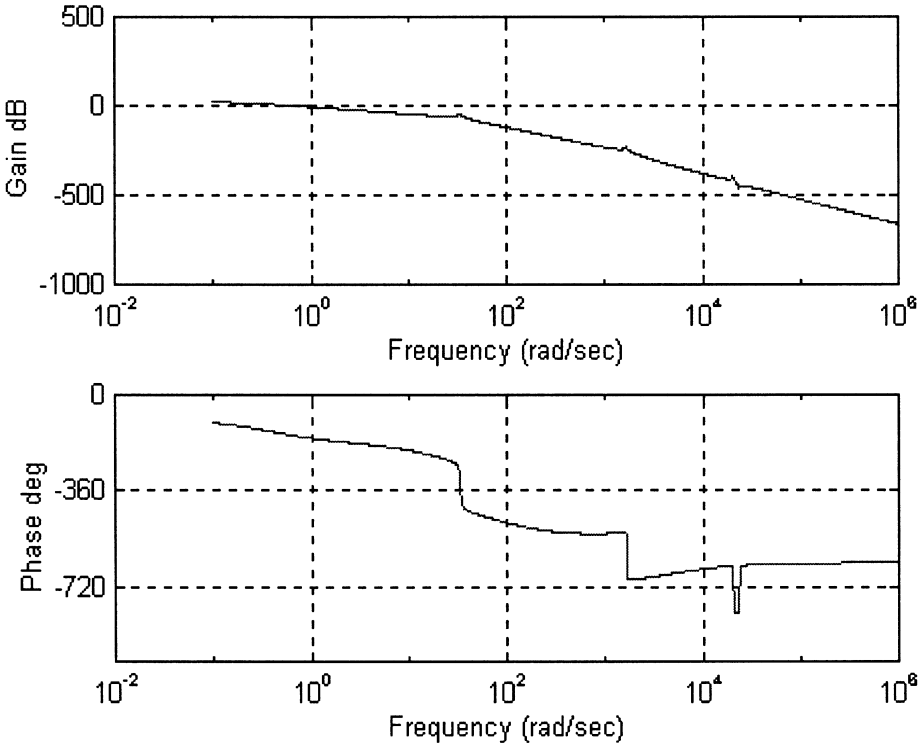

Fig. 6. Theoretical Bode plot of the supporting structure.

or frequency range would be a better choice. The frequency range to be penalized has been specified by the following transfer function:

$$\frac{e(j\omega)}{u(j\omega)} = r\frac{j\omega\beta+1}{j\omega\alpha+1} \tag{5}$$

where r is scalar multiplier and e is the input to the frequency reshaping filter. In state space form, the filter is given by

$$\dot{z} = -\frac{1}{\alpha}z + \frac{r\beta}{\alpha}u$$
$$e = \left(\frac{1}{\alpha} - \frac{1}{\beta}\right)z_2 + \frac{r\beta}{\alpha}u \tag{6}$$

where z is the state of the filter. To give an extra penalty to high frequency u compared to low-frequency u, the following is maintained: $\beta > \alpha > 0$. The plant and filter state equations, (3) and (6), are combined to form an augmented plant:

$$\begin{bmatrix} \dot{z} \\ \dot{\mathbf{x}} \end{bmatrix} = \boldsymbol{A}_e \begin{bmatrix} z \\ \mathbf{x} \end{bmatrix} + \boldsymbol{B}_e e \tag{7}$$

where the extended system and input matrices are

$$\boldsymbol{A}_e = \begin{bmatrix} -\dfrac{1}{\beta} & 0 \\ \dfrac{\boldsymbol{B}}{r}\left(\dfrac{1}{\beta} - \dfrac{\alpha}{\beta^2}\right) & \boldsymbol{A} \end{bmatrix} \quad \text{and} \quad \boldsymbol{B}_e = \begin{bmatrix} 1 \\ \dfrac{\boldsymbol{B}\alpha}{r\beta} \end{bmatrix},$$

respectively. The control is then the conventional one of minimizing for eqn (7) the performance index

$$J = \int_o^\infty [e^2 + qy^2]\,\mathrm{d}t \tag{8}$$

The optimal control is then

$$u = -\boldsymbol{K}_e \begin{bmatrix} z \\ \mathbf{x} \end{bmatrix} = -\boldsymbol{B}_e \boldsymbol{P} \tag{9}$$

where $\boldsymbol{K}_e$ is the gain vector and $\boldsymbol{P}$ is the solution to the steady state Riccati eqn:

$$\mathbf{P}\mathbf{A}_\mathbf{e} + \mathbf{A}_\mathbf{e}^\mathbf{T}\mathbf{P} - (\mathbf{P}\mathbf{B}_\mathbf{e})(\mathbf{P}\mathbf{B}_\mathbf{e})^\mathbf{T} + q\mathbf{C}^\mathbf{T}\mathbf{C} = 0. \tag{10}$$

In the control of IIBM's belt-driven actuator, eqn (1) obtained experimentally has been used as a basis for FRLQ control system design. With the mass position and velocity defined as the two state variables,

$$\mathbf{x} = [x \quad v]$$

the corresponding system and input matrices are

$$\boldsymbol{A} = \begin{bmatrix} 0 & 1 \\ 0 & -25 \end{bmatrix}; \quad \boldsymbol{B} = \begin{bmatrix} 0 \\ 9 \end{bmatrix} \quad \text{and} \quad \boldsymbol{C} = [1 \quad 0].$$

Thus, for the extended matrices defined in eqn (7), the optimal control for the IIBM's first axis is in the form

$$u = -[K_z\ K_x\ K_v] \begin{bmatrix} z \\ \mathbf{x} \end{bmatrix}$$

where the gains are solved from eqns (9) and (10).

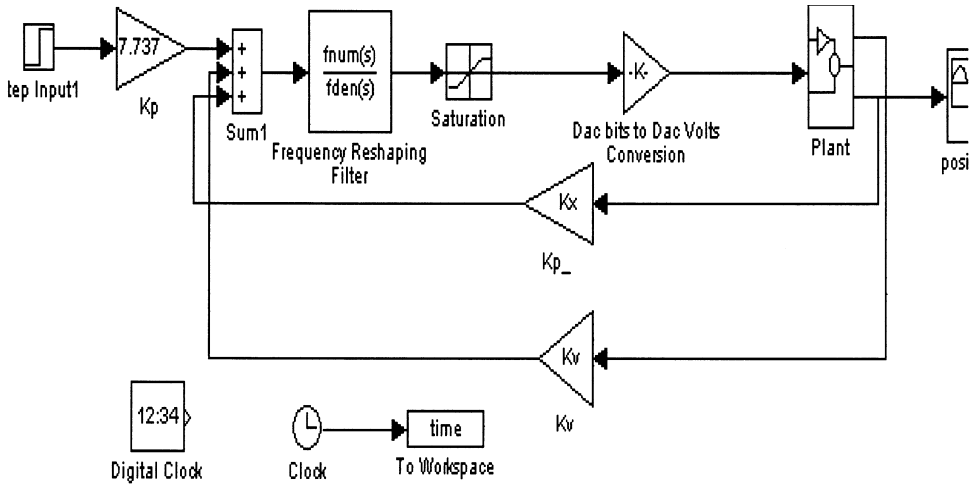

Fig. 7. SIMULINK block diagram of the FRLQ control.

5. Simulation and experimental results

The FRLQ control of the belt-driven actuator has been simulated using MATLAB-SIMULINK® and implemented on the IIBM as shown in Fig. 1. A well-tuned Proportional-Derivative, or PD, control is elected as a basis of comparison since it is a well proven classical controller and is used quite often in industry. The comparison is made to show the improvement FRLQ gives, over an 'industry standard' control method, when high frequency resonances are considered.

The block diagram used in the simulation is shown in Fig. 7 where the 13th order plant model given by eqn (2) is the basis of the test. The filter is chosen to penalize all frequencies above 6 Hz, the frequency at which resonance was first observed. The value of the output weighting was selected after an iterative process to determine the best response in terms of operating time. The control system parameters determined from this control design are given in Table 2.

For experimental implementation purposes, the control algorithms were programmed and downloaded into the memory of the PMAC controller, which utilized its own language for such a purpose. In each test, the system is subjected to a step of

Table 2
Control system parameters

Filter	Gain	Weighting
$\alpha = 0.02$	$K_z = -17.595$	$q = 1000$
$\beta = 0.20$	$K_x = -1.002$	
$r = 1.00$	$K_v = -1.002$	

20,000 encoder counts, the units of length used by the PMAC controller card. This is roughly equivalent to the 22 in performance criteria. No initial conditions were assumed.

Figure 8 shows the simulated step response of the 13th order system with the PD and FRLQ controlled systems, which show a settling time of approximately 0.4 and 0.5 s respectively, and no overshoot. The step responses of the actual IIBM system controlled by the PD and FRLQ control methods are given by Fig. 9. The dynamic responses are similar, and in both cases, satisfy the performance specifications of settling time, overshoot, and steady state error. There is a difference, however, with the system's performance when operated at high frequencies. One way in which the two control designs were tested was by inputting a high amplitude sine wave at the resonance frequency of 36 radians/s in the forward loop and in the feedback loop of the simulated systems.

Figure 10 shows the simulated step response of the system subjected to sinusoidal noise superimposed in the position signal. The amplitude of this noise is 10,000 encoder counts. In the steady state, the position of the mass oscillates around its regulated point. This 'steady-state oscillation' has, for the PD controlled system, amplitude of 2000 encoder counts. The FRLQ controlled system, though, exhibits a more damped oscillation, having amplitude of 500 encoder counts. This result is also true for the case when the noise is input in the forward path, between the filter and the plant. The FRLQ controlled system reduces the simulated resonance by 75% over PD control.

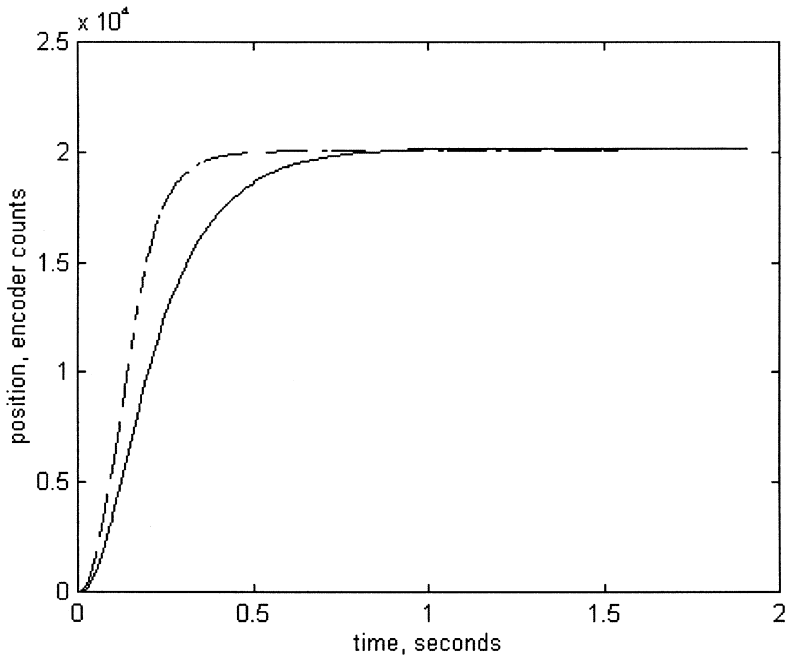

Fig. 8. Simulated step response of PD and FRLQ control (solid line-FRLQ; dashed line—PD).

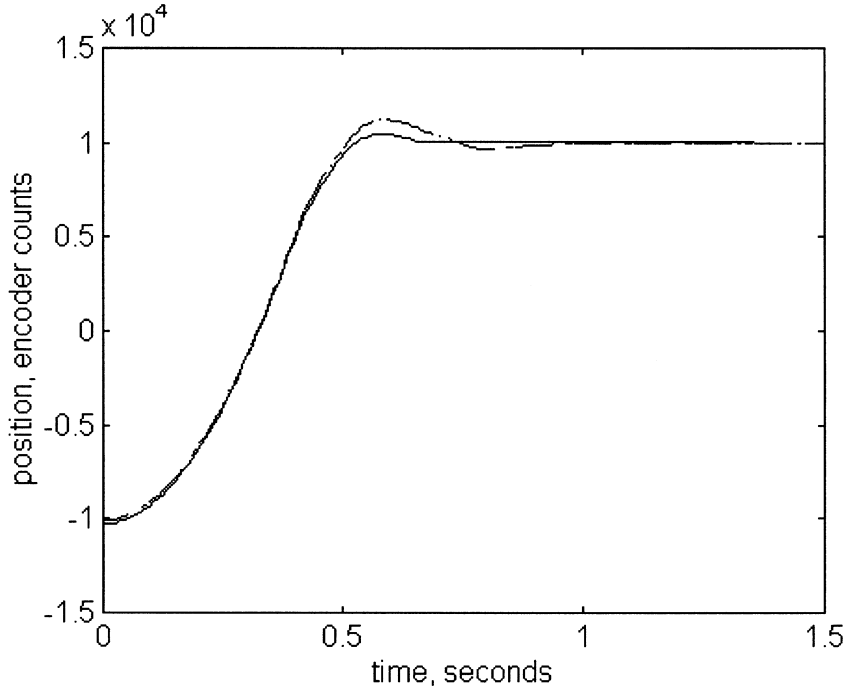

Fig. 9. Experimental step response of PD and FRLQ control (solid line-FRLQ; dashed line—PD).

For the real-world test, we created a sinusoidal disturbance in the forward loop and commanded the system to keep its starting position. Hence, the simulation is in step with the feedback resonance and the experimental test is a regulation of no change with forward-loop disturbance. Another test was conducted on the actual system. For each type of control, a sine wave disturbance with amplitude of 10,000 encoder counts was input to the system that was commanded to keep its starting position. As shown in Fig. 11, the FRLQ controlled system exhibited oscillations that were approximately half as large in amplitude as those from a PD controlled system.

7. Conclusions and future work

The dynamic model and the control strategy have been developed for a belt-driven robot. The control strategy, based on the FRLQ method, has been implemented on the first axis of an IIBM. The performance has been evaluated analytically by simulation and experimentally, the results of which are compared against a well-tuned PD controller. PD control, though a well proven type of control in industry, does not perform well when the system is subjected to high noise frequencies. The reason for this comparison is to show the improvement FRLQ gives, over an 'industry standard' control method, when high frequency resonances are considered.

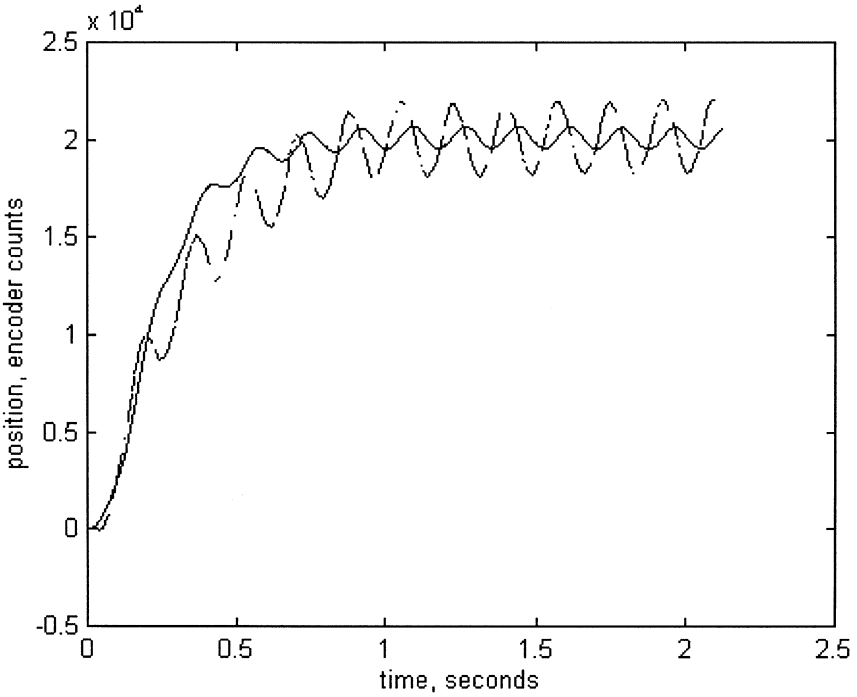

Fig. 10. Simulated step response, system subjected to sensor noise (dashed line—PD; solid line-FRLQ control).

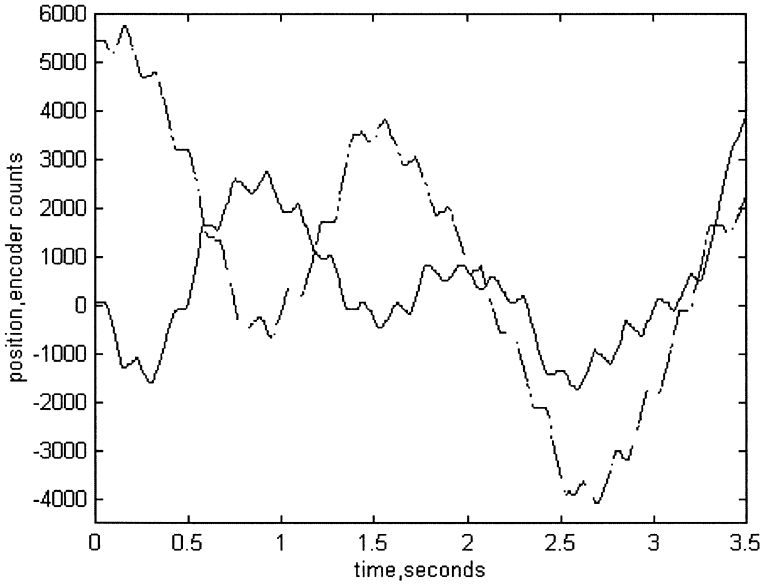

Fig. 11. Actual step response, system subjected to input noise (dashed line—PD; solid line-FRLQ control).

One drawback with FRLQ control is that the harmful frequency or frequencies must be known prior to control, because the FRLQ method is very dependent on what frequencies are penalized. The noise frequencies were estimated using both theoretical models, and the 6 Hz resonance was verified experimentally. The higher frequency resonances were not experimentally verified for safety reasons. The control for the IIBM therefore penalized all frequencies above 6 Hz, to take into account any possible resonance above this. The simulated system was constructed using ideal elements, and therefore garnered slightly different results from the actual system. One of the factors contributing to this difference was the presence of coulomb friction between the lumped mass and the structure via the linear bearing. Another possible discrepancy was the estimation of the structure parameters. Even with these differences, it is easy to see the effect of FRLQ control on the belt-driven system. When subjected to noises, this type of control improved the steady-state performance over the PD controlled system with input noise by no less than 50%. This improvement was accomplished by the introduction of a simple first-order filter on the input. It is speculated that filters of a higher order could improve the steady state performance of the system even more. The implementation of such filters is left as the subject of future work.

Acknowledgements

This project is partially supported by the GTRI Agricultural Technology Research Program and by NSF DUE-945388.

References

[1] Daley W et al. Robotics in meat, fish and poultry processing. In: Khodabandhloo K, editor. Suffolk, U.K.: Blackie Academic and Professional, 1993.
[2] McMurray G, Rutherford C, Piepmier J, Biro R, Holcombe W, Lee K-M. Automation in the poultry industry: the application of human-level performance robotics. IEEE/ASME AIM'97, Tokyo, Japan, June 16–20, 1997.
[3] Mills JK. Control of robotics manipulators with flexible joints during constrained motion task execution. In: Proceedings of the 28th Conference on Decision and Control, Tampa, Florida, December 1989. pp. 1676–1681.
[4] Wang W-S, Liu C-H. Implementation of H_2 optimal controller for a single link flexible-joint robot. In: Proceedings of 1990 IEEE International Conference on Robotics and Automation, 1990. pp. 1438–1443.
[5] Gupta NK. Frequency-shaped cost functionals: extension of linear-quadratic-gaussian design methods. J. of Guidance and Control 1980;3:529–35.
[6] Anderson BDO, Moore JB. Linear optimal control. Englewood Cliffs, NJ: Prentice-Hall, 1971.
[7] Imai H, Abe N, Makoto K. Disturbance attenuation by a frequency-shaped linear-quadratic-regulator method. J of Guidance and Control 1986;9:397–402.